THE JOURNAL OF PHYSICAL CHEMISTRY C

Article

Cite This: J. Phys. Chem. C 2018, 122, 12029−12037

pubs.acs.org/JPCC

Palladium Carbide and Hydride Formation in the Bulk and at the Surface of Palladium Nanoparticles

Aram L. Bugaev,*[,†,‡] Oleg A. Usoltsev,[†] Alexander A. Guda,[†] Kirill A. Lomachenko,[†,§] Ilia A. Pankin,[†,‡] Yuri V. Rusalev,[†] Hermann Emerich,[§] Elena Groppo,[‡] Riccardo Pellegrini,[∥] Alexander V. Soldatov,[†] Jeroen A. van Bokhoven,[#] and Carlo Lamberti*[,†,⊥]

[†]The Smart Materials Research Center, Southern Federal University, Sladkova 174/28, 344090 Rostov-on-Don, Russia

[‡]Department of Chemistry and NIS Interdepartmental Centre, University of Turin, Via P. Giuria 7, 10125 Turin, Italy

[§]European Synchrotron Radiation Facility, 71 avenue des Martyrs, CS 40220, 38043 Cedex 9 Grenoble, France

[∥]Chimet SpA - Catalyst Division, Via di Pescaiola 74, 52041 Viciomaggio Arezzo, Italy

[#]Institute for Chemical and Bioengineering, ETH Zurich, Switzerland and Laboratory for Catalysis and Sustainable Chemistry, Paul Scherrer Institute, Vladimir-Prelog-Weg 1, 8093 Zurich, 5232 Villigen, Switzerland

[⊥]Department of Physics, INSTM Reference Center and CrisDi Interdepartmental Centre for Crystallography, University of Turin, Via P. Giuria 1, 10125 Turin Italy

Supporting Information

ABSTRACT: The presence of a core/shell behavior in Pd nanoparticles (NPs) during the formation of the metal-hydride phase has recently been highlighted combining X-ray absorption and scattering experiments [*J. Phys. Chem. C* **2017**, *121*, 18202]. In this work, we focus on the formation of the carbide phase in the bulk region and on the surface of supported palladium NPs because it affects the catalytic activity and selectivity in hydrogenation reactions. We present *in situ* X-ray absorption spectroscopy study of carbide formation and decomposition in 2.6 nm palladium nanoparticles supported on carbon during exposure to acetylene, hydrogen, and their mixtures at 100 °C, taken as a representative temperature for hydrogenation reactions. Fourier analysis of extended X-ray absorption fine structure (EXAFS) spectra was used to determine the average Pd−Pd bond distance in the NPs, reflecting the formation of bulk palladium carbide, while theoretical calculation of X-ray absorption near-edge structure (XANES) using the finite difference method allowed us to determine the PdC_y stoichiometry in the bulk region and at the surface of the nanoparticles. The difference in the XANES and EXAFS results indicated different behavior of bulk and surface carbide formation. In particular, exposure to pure acetylene leads to the immediate formation of surface Pd−C bonds and much slower growth of bulk carbide, resulting in the increase of Pd−Pd bond distance with respect to pure metallic palladium nanoparticles by only ∼0.6% after 1 h of exposure. Vacuum conditions at 100 °C did not affect the carbide structure of both the bulk and surface of the NPs. However, exposure to H_2 at 100 °C cleans the surface of palladium, removing surface Pd−C bonds, without decomposing bulk carbide. After second exposure to acetylene, this fraction of lost Pd−C bonds is immediately restored, and the bulk carbide phase continues growing. Thus, we showed how the combination of near-edge and extended structures of the absorption spectra can be utilized to determine the properties of surface and bulk regions of palladium nanoparticles, which showed different behavior in formation of the Pd−C bonds.

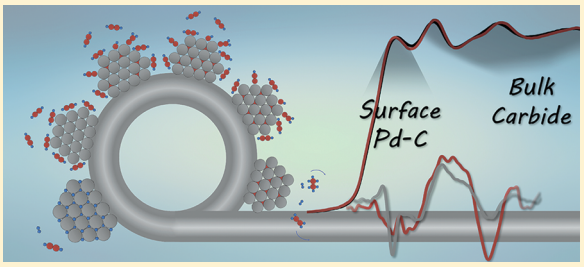

1. INTRODUCTION

Palladium-based materials are extensively exploited as catalysts in the petrochemical industry for selective hydrogenation of hydrocarbons.[1−7] In reaction conditions a phase transition from metallic palladium to one of its hydrides[8−17] or carbides[8,16,18,19] may occur, which affects the catalytic activity and selectivity of material.[18,20] While the phase diagram of palladium hydride is well-studied for both bulk[21] and nanoparticles (NPs),[12,17,21b,22,23] structure, properties, and formation conditions of palladium carbide phases are still poorly understood.[8,18,19,24]

Upon formation of palladium hydride or carbide phases, hydrogen or carbon atoms occupy octahedral interstitial sites of the fcc lattice of palladium, increasing the lattice parameter, which was widely investigated by X-ray powder diffraction (XRPD)[16,17,25,26a] and extended X-ray absorption spectroscopy (EXAFS)[8,16,17,19,26,27,28] studies. However, as we have shown in our previous work,[16] neither of these methods allows us to unambiguously distinguish between hydride and carbide phases, which makes them ineffective in determination of the active palladium phase in reaction conditions. Indeed, in the earliest

Received: November 21, 2017
Revised: February 13, 2018
Published: February 28, 2018

DOI: 10.1021/acs.jpcc.7b11473
J. Phys. Chem. C 2018, 122, 12029−12037

XRPD studies of the catalytic reactions over supported Pd NPs, Bragg peaks due to the carbide phase were improperly assigned to the hydride phase.[29−31]

The direct experimental detection of PdC_y and PdH_x phases can be done discriminating the electronic states appearing in the formation of Pd−C or Pd−H bonds, due to mixing of Pd orbitals with those of carbon or hydrogen ligands, respectively. In particular, X-ray photoelectron spectroscopy (XPS) was successfully applied to determine surface PdC species formed during hydrogenation of alkynes and alkenes over palladium.[18,32] The formation of new antibonding states in palladium hydride[9,33] and carbide[19,24] phases has been revealed by means of Pd L_3-edge (E = 3173 eV) X-ray absorption near-edge structure (XANES) spectroscopy.[34] We have shown that similar information can be extracted from the Pd K-edge (E = 24350 eV) XANES,[16,35] the big advantage of which is that utilization of hard X-rays is much more suited for *in situ* and *operando* investigation of the catalysts.

In the present study, we investigate carbide formation and decomposition in the bulk and on the surface of supported 2.6 nm palladium nanoparticles upon their exposure to acetylene, hydrogen, and their mixtures, by means of Pd K-edge EXAFS and XANES spectroscopies.[34,36] An accelerated version of FDMNES code[37,38] was applied to perform theoretical XANES calculations for metallic Pd, PdH_x, and PdC_y structures optimized by density functional theory (DFT). Numerical fitting of experimental spectra by theoretical ones within the multidimensional interpolation approach indicates that exposure of the sample to hydrogen-containing catalytic mixtures results in formation of the PdH phase; however, in pure acetylene, a surface Pd−C layer forms immediately, and the bulk PdC phase grows gradually, resulting after 1 h of exposure in the increase of the Pd−Pd bond distance by only 0.6% with respect to pure palladium. We found that this bulk carbide is formed irreversibly and is not decomposed at 100 °C both in vacuum conditions and in pure H_2, which is in agreement with previous studies.[16,19] However, the fraction of surface Pd−C bonds, formed due to adsorption of hydrocarbon molecules, can be easily removed by exposure of the sample to H_2 at 100 °C with subsequent evacuation. This procedure leads to a considerable decrease of the number of Pd−C bonds in the sample, as determined by XANES analysis.

2. MATERIALS AND METHODS

2.1. Material Characterization. In this work, we use industrial 5% Pd/C catalyst provided by Chimet S.p.A (http://www.chimet.com/public/download/rd_kit.pdf, product number D1190) consisting of palladium nanoparticles with average size of D = 2.6 nm determined by transmission electron microscopy (TEM) and narrow size distribution with standard deviation determined by Gaussian fitting σ = 0.4 nm. The particles are supported on the wood-based activated carbon with surface area of 980 $m^2\ g^{-1}$ and pore volume of 0.62 $cm^3\ g^{-1}$.[39] The catalyst was dried overnight prior to XAS measurements. Detailed TEM, XRPD, and EXAFS characterization of the sample is reported in our previous work.[17]

2.2. Experimental X-ray Absorption Spectroscopy. Experimental X-ray absorption spectra were collected at the BM31 beamline of the European Synchrotron Radiation Facility (Grenoble, France).[40] The sample powder was stored inside a 1.5 mm thick glass capillary connected to a vacuum line that allowed us to control partial pressures of acetylene and hydrogen inside the capillary. Temperature was controlled by means of the gas blower. To remove surface oxide from the nanoparticles, the sample was activated at 125 °C in hydrogen prior to XAS measurements. Pd K-edge spectra were acquired in transmission mode in the energy range of 24.1−25.4 keV using ionization chambers and a double-crystal Si(111) monochromator detuned to 80% in the continuous scanning mode. The time per one measurement was about 15 min. Using a third ionization chamber,[41] simultaneous measurements of palladium foil were performed for energy calibration.

2.3. EXAFS Analysis. A single-shell Fourier approach was applied for EXAFS data analysis. Background subtraction, normalization, energy alignment, and extraction of $\chi(k)$ oscillatory functions were performed in the Athena program of the Demeter package.[42] Further analysis in the Artemis program included calculation of theoretical amplitudes and phases by the FEFF6 code[43] and first-shell fitting in the R-range from 1.5 to 3.0 Å of the Fourier-transformed data k^2-weighted $\chi(k)$ applying Δk window from 5.0 to 12.0 $Å^{-1}$ with the width of the window slope dk = 1 $Å^{-1}$. The lower limit of the Fourier transform region was chosen as high as 5.0 $Å^{-1}$ to neglect the Pd−C contribution in the first-shell EXAFS analysis. The fitting parameters were the first-shell Pd−Pd interatomic distance (R_{Pd-Pd}), Debye−Waller factor (σ^2), zero energy shift (ΔE_0), and first-shell coordination number (N). The passive electron reduction factor S_0^2 = 0.83 was obtained by fitting the spectra of the palladium foil and kept fixed to determine reduction of coordination numbers in the nanoparticles which was consistent with the average nanoparticle size.

2.4. Optimization of PdH_x and PdC_y Structures. Geometries of PdH_x and PdC_y structures were optimized in VASP 5.3 code[44−46] using PBE exchange-correlation potential.[47] These calculations do not consider the finite size of palladium particles but were performed to account for structure distortions upon insertion of hydrogen and carbon atoms, which were randomly distributed in octahedral interstitial sites of the fcc supercells containing 32 Pd atoms and different number of H and C atoms corresponding to the H/Pd ratios x of 0, 0.125, 0.250, and 0.500 and C/Pd ratios, y, of 0, 0.0625, 0.1250, and 0.2500. The energy cutoff value for the plane-wave basis was set to 400 eV. The 11 × 11 × 11 Monkhorst-pack grid was used for generation of a k-point mesh, which was tested to provide sufficient convergence of the total energy. The first-order Methfessel−Paxton smearing scheme[48] with smearing width of 0.2 eV was used for relaxation calculations. The convergence criterion for energy difference in SCF cycles and force in geometry relaxation cycles were set to 10^{-5} eV and 10^{-2} eV/Å, respectively. The volume of the supercell was fixed at the values corresponding to the average cell parameter of 3.89, 3.95, and 4.01 Å. These values correspond to average Pd−Pd distances of 2.75, 2.79, and 2.84 Å and correspond to the range from metallic palladium to palladium hydride (x ∼0.6) observed for bulk samples in crystallographic studies.[49] For each structure and for each of the specified cell volumes, relaxation of the atomic positions without symmetry restrictions was performed. The obtained structures are reported in Figure S1 of the Supporting Information.

2.5. XANES Calculation and Fitting. DFT-optimized PdH_x and PdC_y structures were used for XANES calculation by FDMNES code.[37,38,50] Each spectrum, except the pure metallic one, was calculated by averaging 32 separate theoretical spectra for each Pd atom in the optimized supercell. Calculations were performed within the finite difference approach in full potential. A 6 Å cluster around a Pd-absorbing atom was used in all simulations.

DOI: 10.1021/acs.jpcc.7b11473
J. Phys. Chem. C 2018, 122, 12029−12037

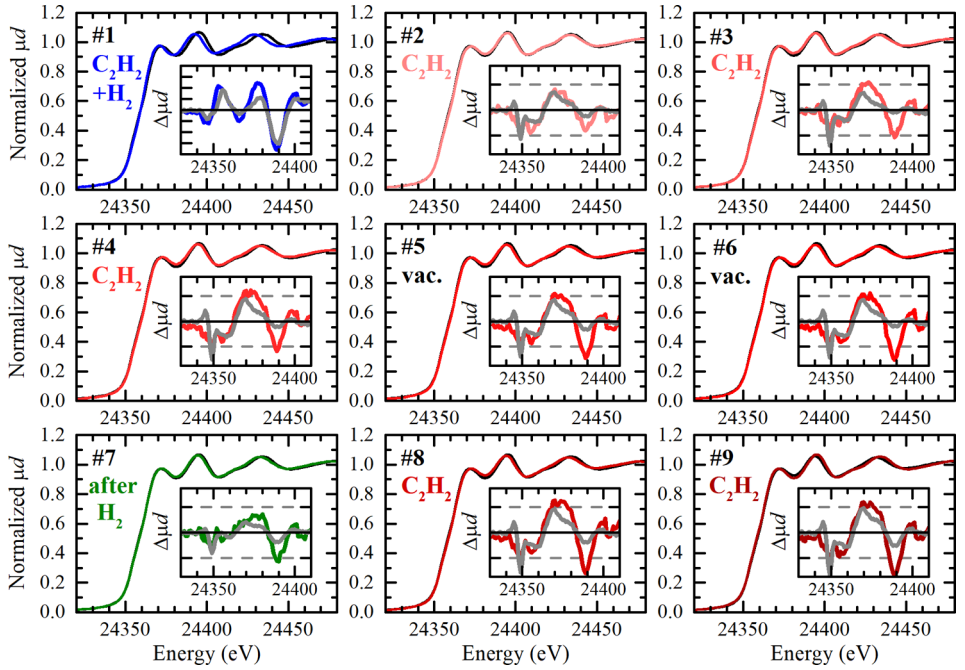

Figure 1. Sequence of XANES spectra of palladium nanoparticles at 100 °C exposed to different conditions (colored lines) reported in Table 1 and plotted together with the spectrum of pure palladium nanoparticles (black lines). The insets show the difference XANES spectra (colored lines) with the theoretical curves (gray lines) obtained as described in Section 3.2. The division interval of the ordinate axes of all insets corresponds to a $\Delta\mu d$ value of 0.02.

Table 1. Details on the Experimental Conditions Adopted for the Collection of the XANES Spectra Reported in Figure 1[a]

#	conditions	contact time	XANES features
0	vacuum	-	pure metallic palladium (black curve in each part of Figure 1)
1	350 mbar C_2H_2 + 650 mbar H_2	-	the first XANES peak at 24360 eV is shifted to lower energy by 1 eV, which indicates hydride formation; all other peaks are also shifted to lower energies due to significant elongation of Pd−Pd distances
2	1000 mbar C_2H_2	15 min	similar to spectrum #0 with small shift of the first peak toward higher energies indicative for carbide phase
3	1000 mbar C_2H_2	30 min	bigger shift of the first peak toward higher energies, indicating further growth of the carbide phase; small shift of all other peaks to lower energies due to small elongation of Pd−Pd distances
4	1000 mbar C_2H_2	50 min	further growth of carbide phase
5	vacuum	15 min	no considerable changes with respect to spectrum #4
6	vacuum	30 min	no considerable changes with respect to spectrum #4
-	H_2-treatment	-	sample was exposed to H_2 for 5 min and then evacuated to 10^{-3} mbar
7	vacuum	-	after H_2 treatment, the first XANES peak almost coincides with those of spectrum #0 indicating partial decomposition of carbide; but the shift of all other peaks is still present as in spectra #4−6, which means that the Pd−Pd distances are still elongated with respect to pure palladium nanoparticles.
8	1000 mbar C_2H_2	15 min	spectrum has similar features as in spectrum #4, indicating that the fraction of decomposed palladium carbide is formed again
9	1000 mbar C_2H_2	30 min	further growth of palladium carbide

[a]All spectra were collected at 100 °C. Also reported is a brief description of the changes observed in the XANES spectra.

Fitting of experimental spectra by theoretical ones was performed by the multidimensional interpolation method implemented in FitIt code.[51,52] Initially calculated spectra for given concentrations x and y in PdH_x and PdC_y (x = 0, 0.125, 0.250, 0.500; y = 0, 0.06, 0.125, 0.250) were used as interpolation nodes to obtain spectra for all intermediate concentrations. To exclude systematic errors and increase precision, fitting was performed for difference XANES spectra. To plot the experimental difference spectra, we subtracted a spectrum of initial metallic palladium nanoparticles measured in vacuum from all other spectra, while the theoretical ones were obtained after subtracting the fitted theoretical spectrum of metallic palladium nanoparticles.

3. RESULTS

3.1. Experimental X-ray Absorption Spectra. The evolution of the atomic structure of the palladium catalyst during exposure to acetylene and hydrogen was followed by *in situ* measuring of Pd *K*-edge XAS spectra. All experimental spectra are shown in Figure 1, while the adopted conditions and brief description of each spectrum are reported in Table 1.

Initially the sample was activated in pure H_2 at 120 °C, successively evacuated, and cooled to 100 °C to obtain the spectrum of the clean nanoparticles (spectrum #0 in Table 1 and black curve in each part of Figure 1). Then the sample was exposed to a mixture of acetylene and hydrogen with partial pressures of 350 and 650 mbar, respectively, and spectrum #1

DOI: 10.1021/acs.jpcc.7b11473
J. Phys. Chem. C 2018, 122, 12029−12037

was acquired. The shape of the XANES region (Figure 1, spectrum #1) indicated that in a H_2/C_2H_2 mixture the palladium nanoparticles have the hydride phase, close to that obtained in pure hydrogen at similar temperature and pressure regimes.[14,16] After 15 min, the pressure in the closed experimental cell had dropped from 1000 to 925 mbar. The observed pressure drop indirectly testifies the hydrogenation of acetylene because formation of one ethylene molecule from one hydrogen and one acetylene decreases the total number of molecules in the closed cell. In addition, it should be noted that the process of hydride formation is fast,[53] and the initial pressure of 1000 mbar was measured when the hydride phase had already been formed. To form the palladium carbide phase, we then exposed the sample to pure acetylene, and three consecutive XAS spectra (#2, #3, and #4 in Figure 1) were taken. The stability and reversibility of the carbide phase were checked first by evacuation down to 10^{-3} mbar at 100 °C (spectra #5 and #6) and then by treatment in hydrogen (1000 mbar at 100 °C) with subsequent evacuation (spectrum #7). Then, the sample was exposed again to pure acetylene, and the last two spectra at 100 °C (#8 and #9) were collected. To better highlight the changes in XANES spectra, difference spectra (insets in Figure 1) were obtained by subtracting from each of the spectra the one of the pure palladium nanoparticles (spectrum #0, black curve).

As we have demonstrated in our previous work,[16] palladium hydride and carbide phases have characteristic XANES features, which allow performing a qualitative analysis of the PdH_x or PdC_y stoichiometry. The main changes in the XANES features along these experiments are summarized in Table 1. Initially, in a mixture of hydrogen and acetylene the dominant phase is palladium hydride (Figure 1, spectrum #1), which is different from all other spectra in the series. The immediate appearance of Pd−C features is observed when the sample is exposed to pure acetylene. In the spectra #3 and #4 these features are becoming even stronger indicating that the carbide phase is forming progressively with time. No considerable spectral changes (Figure 1, spectra #5 and #6) were observed in subsequent vacuum conditions, which means that the formed carbide phase does not decompose under vacuum. However, after the sample was treated in hydrogen, the shape of difference XANES spectra (#7 in Figure 1) changed back toward a lower amount of carbide features, suggesting that Pd−C species can be partially removed by treatment in H_2 at 100 °C. Upon renewed exposure to acetylene these features in the spectra return back to the same level as detected before treatment in H_2 and continue to grow (spectra #8 and #9 in Figure 1).

3.2. XANES and EXAFS Analysis. To quantify the changes described in the previous paragraph, the XAS spectra were analyzed following two independent routes. First, a standard first-shell Fourier analysis of the EXAFS region was performed to obtain the evolution of Pd−Pd distance and other structural parameters, reported in Table 2 (theoretical and experimental $\chi(k)$ functions, and their Fourier transforms are reported in Figure S2). Second, for each experimental XANES spectrum, the relative carbon stoichiometry, y, and the average R_{Pd-Pd} distance were determined on the basis of the best agreement with the library of theoretical XANES spectra obtained with the interpolation method (vide infra).

The geometrical models used for the XANES calculations represented supercells containing 32 palladium atoms (Figure S1). Part of the octahedral interstitial sites formed by the palladium lattice was occupied by carbon atoms, resulting in the C/Pd ratios, y, changing from 0.00 to 0.25. Palladium hydride structures were also considered with H/Pd ratios, x, changing from 0.00 to 0.50. These structures were further optimized using VASP code as described in Section 2.4. This approach does not consider the finite size of the nanoparticles but allows us to account for structure distortions in palladium carbide and hydride nanoparticles induced by carbon and hydrogen incorporation, respectively, which is important because according to EXAFS data the formation of hydride[17] and carbide (Table 2) phases increases the local disorder reflected in the bigger Debye−Waller parameter in comparison with pure palladium.

Table 2. Structural Parameters Obtained from First-Shell Analysis of EXAFS Data and Concentration y of Carbon Atoms of the PdC_y (x of PdH_x Phase Is Reported for Spectrum #1) Phase Determined by XANES Fitting (Performed Fixing R_{Pd-Pd} to the Value Optimized in the EXAFS Analysis), Last Column[a]

	EXAFS fit			XANES fit
#	R_{Pd-Pd}, Å	σ^2, Å^2	E_0, eV	y
0	2.739 ± 0.004	0.0073 ± 0.0002	24353.2 ± 0.9	-
1	2.812 ± 0.004	0.0090 ± 0.0002	24353.4 ± 0.8	x = 0.35
2	2.747 ± 0.004	0.0083 ± 0.0002	24353.2 ± 0.9	0.044
3	2.748 ± 0.009	0.0088 ± 0.0004	24352.1 ± 1.8	0.043
4	2.754 ± 0.008	0.0090 ± 0.0003	24352.6 ± 1.6	0.051
5	2.755 ± 0.009	0.0091 ± 0.0004	24352.4 ± 2.0	0.050
6	2.751 ± 0.008	0.0094 ± 0.0004	24352.0 ± 1.7	0.050
7	2.759 ± 0.005	0.0085 ± 0.0002	24353.4 ± 1.0	0.024
8	2.752 ± 0.007	0.0092 ± 0.0003	24351.3 ± 1.6	0.054
9	2.754 ± 0.011	0.0095 ± 0.0005	24351.3 ± 2.2	0.055

[a]In the EXAFS fit, the coordination, N, was determined as 10.0 ± 0.9 for bare palladium and then kept fixed at N = 10 for all spectra #1 − #9.

The optimized structures were used for XANES calculation using the full potential finite difference approach.[50] Since due to the induced distortions different palladium atoms in the supercell are no longer equivalent, for each structure (except for the pure palladium one) 32 independent XANES calculations were performed and then averaged. As a result, each of the theoretical spectra can be characterized by two independent parameters, which describe the original atomic structure: (1) the average Pd−Pd interatomic distance (R_{Pd-Pd}), derived from the volume of the supercell, and (2) relative concentration y and x of carbon and hydrogen atoms, respectively. Calculated spectra represent a 2-dimentional grid of these parameters with R_{Pd-Pd} equal to 2.75, 2.79, and 2.83 Å, concentration of carbon atoms y equal to 0.0000, 0.0625, 0.1250, and 0.2500, and concentration of hydrogen atoms x equal to 0.000, 0.125, 0.250, and 0.500 (see Figure 2a). The effect of each parameter on the shaping of difference XANES spectra is demonstrated in Figure 2b−f. Using the multidimensional interpolation approach,[51] these calculated spectra were used to predict any spectrum corresponding to any point on the (R_{Pd-Pd}, y) plane, and these data were used to fit the experimental spectra. During the fitting procedure, the R_{Pd-Pd} parameter was always set to the value determined by the first-shell EXAFS analysis, while the carbon (hydrogen) concentration was varied to minimize the root-mean-square deviation between experimental and theoretical difference XANES, where experimental difference spectra were constructed by subtracting a spectrum of metallic palladium nanoparticles in vacuum and the theoretical ones by subtracting the spectrum of pure Pd with R_{Pd-Pd} = 2.74 Å as in metallic palladium nanoparticles. During the fitting procedure, we also

DOI: 10.1021/acs.jpcc.7b11473
J. Phys. Chem. C 2018, 122, 12029−12037

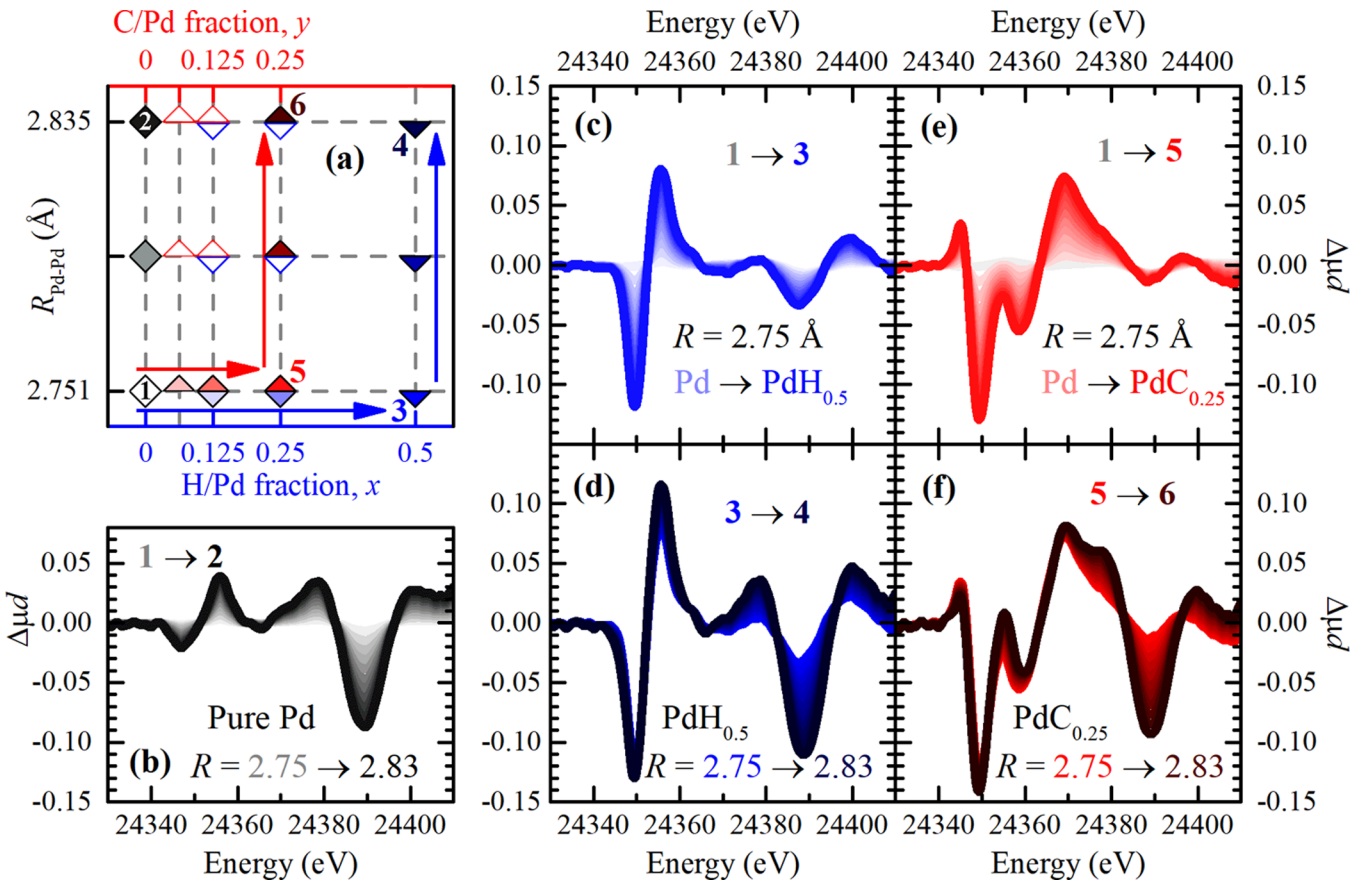

Figure 2. (a) Representation of the structure−stoichiometry planes R_{Pd-Pd}-x (left and bottom axes) and R_{Pd-Pd}−y (left and top axes) for hydride and carbide phases, respectively, investigated in the XANES simulations. Up- and down-triangles represent the points in the structure−stoichiometry planes where the XANES spectra of hydrides and carbides, respectively, have been calculated by FDMNES on VASP optimized structures. Diamonds correspond to pure Pd. The color filling of selected scatters indicates the interpolation nodes used to obtain spectra presented in parts (b−f). For all other scatters, only border color is used. (b−f) Demonstrate the effect of structural and stoichiometric changes on the theoretical difference XANES spectra. The spectrum of pure Pd with R_{Pd-Pd} = 2.74 Å has been used in all subtractions. (b) Effect of the variation of R_{Pd-Pd} from 2.75 (light gray) to 2.83 Å (black) in the pure metal phase ($x = y = 0$). (c) Effect of the variation of the hydrogen concentration x in the PdH_x from 0 (light blue) to 0.5 (blue) at R_{Pd-Pd} = 2.75 Å. (d) Effect of R_{Pd-Pd} increase from 2.75 Å (blue) to 2.83 Å (dark blue) at x = 0.5. (e) Effect of the variation of the carbon concentration y in the PdC_y from 0 (light red) to 0.25 (red) at R_{Pd-Pd} = 2.75 Å. (f) Effect of R_{Pd-Pd} increase from 2.75 Å (red) to 2.83 Å (dark red), y = 0.25.

allowed simultaneous variation of both Pd−H and Pd−C fractions as two fitting parameters. This resulted in negative values of Pd−C fraction for spectrum #1 and small and negative values of Pd−H fraction for spectra #2−9 (see Figure S4), indicating that in palladium NPs, under the adopted experimental conditions, the formation of one of these phases excludes formation of another.

3.3. Carbide Formation in the Bulk and at the Surface of the Nanoparticles. Spectra #0 and #1 correspond to the pure metallic and hydride phase of the palladium NPs, respectively. Formation of Pd−C bonds occurs, when the catalyst is exposed to pure acetylene at 100 °C resulting in well-pronounced carbide-like[16] features already in spectrum #2 of Figure 1. However, the determined R_{Pd-Pd} value is very close (the relative change is below 0.3%) to that of pure metallic palladium (Figure 3), and if the amount of carbon atoms determined by XANES (∼5%) was really incorporated inside the palladium lattice, they should have caused much stronger elongation of R_{Pd-Pd}. In particular, XRPD studies revealed that lattice expansion in palladium black upon carbide phase formation is 2.6%. This seeming contradiction is explained by assuming that the Pd−C contribution that changes the shape of the XANES

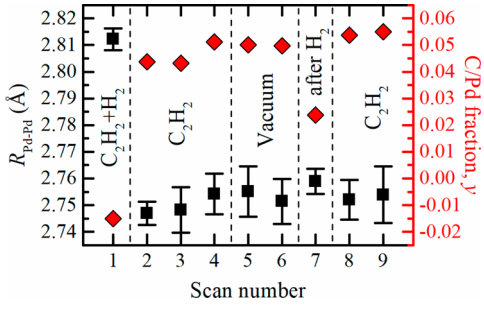

Figure 3. Evolution of R_{Pd-Pd} obtained from the first-shell EXAFS analysis (black squares, left axis) and stoichiometry of the PdC_y phase determined by XANES fitting (red diamonds, right axis).

spectra mainly originates from acetylene molecules adsorbed at the surface of the palladium nanoparticles. These adsorbed molecules make a considerable contribution to spectra due to the small particle size (2.6 nm in diameter). The further small increase of interatomic distances and the concentration of carbon atoms along spectra #3 and #4 (Figure 3) are explained by decomposition of acetylene to carbon and diffusion of these carbon atoms to the core of the nanoparticles, the process that takes

DOI: 10.1021/acs.jpcc.7b11473
J. Phys. Chem. C 2018, 122, 12029−12037

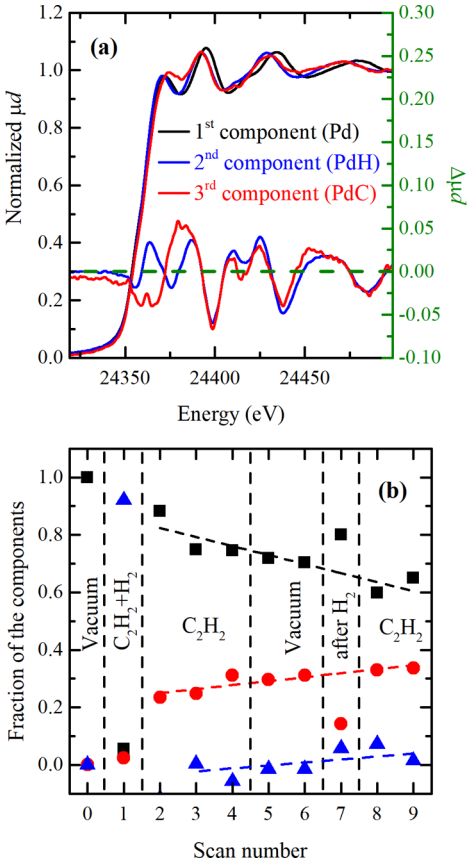

Figure 4. (a) Components determined by PCA (reconstructed after vector rotation) which correspond to pure metallic (black), hydride (blue), and carbide (red) phases of palladium. The corresponding difference spectra are presented in the enlarged scale shown in the right axis. (b) Evolution of metal, hydride and carbide phases (black squares, blue triangles and red circles, respectively), obtained by PCA along the different sample treatments.

place at longer time scales. The obtained values of R_{Pd-Pd} and y do not change in vacuum (10^{-3} mbar) conditions (spectra #5 and #6), indicative of stable bulk and surface carbide.

Successively, 1000 mbar of H_2 has been dosed to the sample at 100 °C and removed after 5 min of contact, and spectrum #7 was collected in a dynamic vacuum (10^{-3} mbar), indicating a double decrease of the C/Pd stoichiometry from $PdC_{0.050}$ to $PdC_{0.024}$ but the same R_{Pd-Pd} with respect to spectra #4–#6. The stability of the R_{Pd-Pd} values obtained from EXAFS indicates that the H_2 treatment at 100 °C does not affect the structure of the bulk carbide phase. At the same time, a significant decrease of carbon concentration observed in XANES is explained by removal of the surface Pd–C bonds. This process is most probably accompanied by hydrogenation of the adsorbed carbon-containing species (vide infra) and their subsequent removal from the catalyst surface. Such results imply that treatment in hydrogen allows us to clean the surface of the nanoparticles from adsorbed hydrocarbon molecules. After the second exposure to pure acetylene (spectra #8 and #9 in Figure 1) the lost fraction y of the PdC_y phase is immediately gained back, as evidenced by the XANES analysis, which means that the Pd–C bonds with surface-adsorbed carbon species are formed again.

The results of the theoretical simulations and fitting of XANES curves were also confirmed by principle component analysis (PCA) of the experimental spectra. The determined number of independent components was equal to 3 (see Section S3 and Figure S5 of the Supporting Information). Then by rotation of the basic vectors[54,55] three main components assigned to pure metallic palladium and its hydride and carbide phases were extracted (Figure 4a). The latter component is not observed in the pure state in any of the experimental conditions, but it should be treated as a theoretical extrapolation, corresponding to a palladium carbide phase which might be formed after infinitely long exposure to acetylene. It is remarkable that the EXAFS of this component virtually coincides with that of the hydride, meaning that both phases have similar interatomic distances, which correlates with XRPD studies.[16,29,56] The specific carbide feature is only present in the XANES region. After exposure to acetylene, pure metallic and carbide phases coexist in the nanoparticles. At the long time scales the metallic phase has a decreasing tendency, and the opposite trend is observed for the carbide one. After cleaning in hydrogen, the PCA also gives a drop in the Pd–C component and an increase of the pure metallic phase.

The process of hydride and carbide phase formation and decomposition is schematically shown in Figure 5. The most challenging question is the exact composition of the observed surface carbide phase. Acetylene adsorption on palladium surfaces is known to be a complex process which can follow a number of different routes,[57,58] including initially π- and di-σ-adsorption of acetylene and its further transformation to one of the carbon-containing species like vinyl, ethylidyne,[59] ethylidene, and a few others, that are one of the intermediates in the process of acetylene hydrogenation to ethylene and ethane. In addition, complete decomposition to carbon was also reported.[58] The results reported in Figures 3 and 4 demonstrate that XANES spectra are strongly dependent on the presence of carbon-containing deposits on the nanoparticle surface, which escape from being detected by EXAFS analysis. It should be noted, however, that formation of surface and core palladium carbide indirectly affects also the EXAFS region. In particular, the results reported

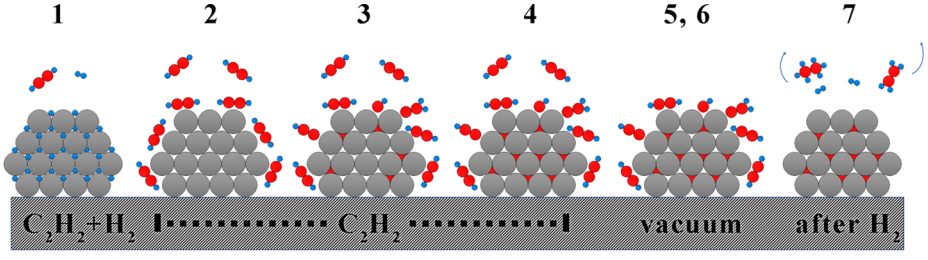

Figure 5. Schematic picture illustrating subsequent palladium hydride formation in the presence of hydrogen and acetylene (1) and decomposition of the hydride phase in pure acetylene, adsorption of acetylene at the surface, and its further decomposition to atomic carbon with formation of bulk carbide (2–4), stability of bulk carbide and surface-adsorbed molecules in vacuum (5, 6), and removal of surface adsorbed molecules by treatment in hydrogen (7).

DOI: 10.1021/acs.jpcc.7b11473
J. Phys. Chem. C 2018, 122, 12029–12037

in the Table 2 for the spectra #2−#9 are characterized by (i) increasing Debye−Waller parameter and (ii) increasing error (except for spectrum 7) in determining R_{Pd-Pd} values. These effects are explained by the coexistence of surface and bulk carbides with different atomic structure, which result in higher static disorder.[17] As we have noted in previous works,[28,60] increases of σ^2 value and R_{Pd-Pd} error are indicating that we have local structure distortion around the Pd atom and/or coexistence of different interatomic distances in the sample, but due to the small difference ΔR_{Pd-Pd} (smaller than 0.01 Å) we were unable to resolve separate Pd−Pd distances for the bulk and shell from EXAFS analysis. The removal of surface carbide leads to a significant decrease of σ^2 and R_{Pd-Pd} error for spectrum #7. In the EXAFS fitting, the lower bound of the Δk interval was intentionally chosen as high as 5 Å^{-1} to minimize the possible contribution of carbon both from the support and from the carbide phase. However, attempts to extend the lower bound of Δk to 2.5 Å^{-1} and to include the Pd−C contribution expected at R from 1 to 2 Å led to meaningless values of the Pd−C coordination number and Debye−Waller parameter. Thus, only XANES analysis is able to provide quantitative information about the carbon atoms. The detection of surface Pd-C phase by XANES has been recentely reported for the in ultra-small Pd NPs[61] formed inside UiO-67 metal-organic framework.[62a,b] In such small NPs, no increase of interatomic distances was observed, however the characteristic XANES features evidenced formation of surface Pd-C.

Although we were not able to determine the exact structure of surface carbon species (e.g., type of the adsorbed molecule and its geometry), the main advantage of the present result is a proof of a possibility to distinguish between bulk and surface carbon species in small nanoparticles using X-ray absorption spectroscopy. Advances in determining the exact type of the adsorbed species can be made utilizing high-energy resolution fluorescence detection (HERFD) XANES[63,64] or Pd L_3-edge XANES, combined with theoretical simulation of the atomic structure.

4. CONCLUSIONS

We demonstrated how simultaneous analysis of *in situ* EXAFS and XANES provides information on the structure in both bulk and surface regions of palladium nanoparticles. This approach was successfully applied to study the formation of a bulk carbide phase and adsorption and desorption of surface carbon species upon exposure of the nanoparticles to acetylene and hydrogen. Exposure to a mixture of acetylene and hydrogen with partial pressures of 350 and 650 mbar, respectively, leads to formation of a hydride phase with no evidence of bulk of surface carbon incorporation. Interaction with pure acetylene leads to rapid formation of carbide features in XANES which is explained by the adsorption of acetylene on the surface of the nanoparticle and its further transformation into other carbon-contacting species. In addition, decomposition of acetylene to carbon induces carbide phase formation in the bulk of the nanoparticles detected via elongation of Pd−Pd distances in EXAFS. The latter process occurs very slowly and results in the bond distance elongation by only ∼0.6% after 1 h of exposure. In agreement with previous reports,[16,19] this bulk carbide is formed irreversibly, at least at the time scales of this study. However, we demonstrated that treatment in hydrogen removes the surface-adsorbed species changing the structure of the nanoparticle surface from a carbide to a metallic one. Adsorption, removal, and reabsorption of these species give a strong contribution to the XANES region, escaping from the detection by EXAFS analysis. Although XANES is mainly sensitive to the formation of Pd−C bonds, it is much more difficult to determine which type of adsorbed carbon species is present. The obtained results demonstrate the principle possibility of discrimination between surface and bulk structures of the nanoparticles by *in situ* and operando XAS, which is important for determining the active phase in the wide range of metal-based nanocatalysts. The present work, in line with other recent advanced studies,[14,16,37,38,54,55,65] highlights how XANES spectroscopy has become a mature technique that, if properly supported by advanced simulations, can provide quantitative structural and stoichiometric analysis of complex systems.

■ ASSOCIATED CONTENT

Supporting Information

The Supporting Information is available free of charge on the ACS Publications website at DOI: 10.1021/acs.jpcc.7b11473.

Visualization of the PdH_x and PdC_y structures, examples of EXAFS fits, and the description of PCA procedure (PDF)

■ AUTHOR INFORMATION

Corresponding Authors

*E-mail: abugaev@sfedu.ru.
*E-mail: carlo.lamberti@unito.it.

ORCID

Aram L. Bugaev: 0000-0001-8273-2560
Alexander A. Guda: 0000-0002-6941-4987
Kirill A. Lomachenko: 0000-0003-0238-1719
Elena Groppo: 0000-0003-4153-5709
Jeroen A. van Bokhoven: 0000-0002-4166-2284
Carlo Lamberti: 0000-0001-8004-2312

Notes

The authors declare no competing financial interest.

■ ACKNOWLEDGMENTS

A.L.B., O.A.U., I.A.P., Yu.V.R., A.A.G., A.V.S., and C.L. acknowledge the Russian Ministry of Education and Science for financial support (Project RFMEFI58417 × 0029, Agreement 14.584.21.0029). We thank the staff of the BM31 beamline of ESRF for the support during XAS measurements. We also thank Mary Bugaeva for preparing the graphical abstract.

■ REFERENCES

(1) Borodziński, A.; Bond, G. C. Selective hydrogenation of ethyne in ethene-rich streams on palladium catalysts. Part 1. Effect of changes to the catalyst during reaction. *Catal. Rev.: Sci. Eng.* **2006**, *48*, 91−144.

(2) Borodziński, A.; Bond, G. C. Selective hydrogenation of ethyne in ethene-rich streams on palladium catalysts, Part 2: Steady-state kinetics and effects of palladium particle size, carbon monoxide, and promoters. *Catal. Rev.: Sci. Eng.* **2008**, *50*, 379−469.

(3) Lazzarini, A.; Piovano, A.; Pellegrini, R.; Leofanti, G.; Agostini, G.; Rudić, S.; Chierotti, M. R.; Gobetto, R.; Battiato, A.; Spoto, G.; et al. A comprehensive approach to investigate the structural and surface properties of activated carbons and related Pd-based catalysts. *Catal. Sci. Technol.* **2016**, *6*, 4910−4922.

(4) Lazzarini, A.; Pellegrini, R.; Piovano, A.; Rudić, S.; Castan-Guerrero, C.; Torelli, P.; Chierotti, M. R.; Gobetto, R.; Lamberti, C.; Groppo, E. The effect of surface chemistry on the performances of Pd-based catalysts supported on activated carbons. *Catal. Sci. Technol.* **2017**, *7*, 4162−4172.

(5) Agostini, G.; Lamberti, C.; Pellegrini, R.; Leofanti, G.; Giannici, F.; Longo, A.; Groppo, E. Effect of pre-reduction on the properties and

the catalytic activity of Pd/carbon catalysts: a comparison with Pd/Al_2O_3. *ACS Catal.* **2014**, *4*, 187−194.
(6) Pellegrini, R.; Agostini, G.; Groppo, E.; Piovano, A.; Leofanti, G.; Lamberti, C. 0.5wt.% Pd/C catalyst for purification of terephthalic acid: Irreversible deactivation in industrial plants. *J. Catal.* **2011**, *280*, 150−160.
(7) Groppo, E.; Agostini, G.; Piovano, A.; Muddada, N. B.; Leofanti, G.; Pellegrini, R.; Portale, G.; Longo, A.; Lamberti, C. Effect of reduction in liquid phase on the properties and the catalytic activity of Pd/Al_2O_3 catalysts. *J. Catal.* **2012**, *287*, 44−54.
(8) McCaulley, J. A. In-situ X-ray absorption spectroscopy studies of hydride and carbide formation in supported palladium catalysts. *J. Phys. Chem.* **1993**, *97*, 10372−10379.
(9) Soldatov, A.; Della Longa, S.; Bianconi, A. Relevant role of hydrogen atoms in the XANES of Pd hydride: Evidence of hydrogen induced unoccupied states. *Solid State Commun.* **1993**, *85*, 863−868.
(10) Kishore, S.; Nelson, J.; Adair, J.; Eklund, P. Hydrogen storage in spherical and platelet palladium nanoparticles. *J. Alloys Compd.* **2005**, *389*, 234−242.
(11) Yamauchi, M.; Ikeda, R.; Kitagawa, H.; Takata, M. Nanosize effects on hydrogen storage in palladium. *J. Phys. Chem. C* **2008**, *112*, 3294−3299.
(12) Langhammer, C.; Larsson, E. M.; Kasemo, B.; Zoric, I. Indirect nanoplasmonic sensing: ultrasensitive experimental platform for nanomaterials science and optical nanocalorimetry. *Nano Lett.* **2010**, *10*, 3529−3538.
(13) Shegai, T.; Langhammer, C. Hydride formation in single palladium and magnesium nanoparticles studied by nanoplasmonic dark-field scattering spectroscopy. *Adv. Mater.* **2011**, *23*, 4409−4414.
(14) Bugaev, A. L.; Guda, A. A.; Lomachenko, K. A.; Srabionyan, V. V.; Bugaev, L. A.; Soldatov, A. V.; Lamberti, C.; Dmitriev, V. P.; van Bokhoven, J. A. Temperature- and pressure-dependent hydrogen concentration in supported PdH_x nanoparticles by Pd K-edge X-ray absorption spectroscopy. *J. Phys. Chem. C* **2014**, *118*, 10416−10423.
(15) Bugaev, A. L.; Guda, A. A.; Lomachenko, K. A.; Bugaev, L. A.; Soldatov, A. V. Pd hydride and carbide studied by means of Pd K-edge X-ray absorption near-edge structure analysis. *Bull. Russ. Acad. Sci.: Phys.* **2015**, *79*, 1180−1185.
(16) Bugaev, A. L.; Guda, A. A.; Lazzarini, A.; Lomachenko, K. A.; Groppo, E.; Pellegrini, R.; Piovano, A.; Emerich, H.; Soldatov, A. V.; Bugaev, L. A.; et al. In situ formation of hydrides and carbides in palladium catalyst: when XANES is better than EXAFS and XRD. *Catal. Today* **2017**, *283*, 119−126.
(17) Bugaev, A. L.; Guda, A. A.; Lomachenko, K. A.; Shapovalov, V. V.; Lazzarini, A.; Vitillo, J. G.; Bugaev, L. A.; Groppo, E.; Pellegrini, R.; Soldatov, A. V.; et al. Core−shell structure of palladium hydride nanoparticles revealed by combined X-ray absorption spectroscopy and X-ray diffraction. *J. Phys. Chem. C* **2017**, *121*, 18202−18213.
(18) Teschner, D.; Borsodi, J.; Wootsch, A.; Revay, Z.; Havecker, M.; Knop-Gericke, A.; Jackson, S. D.; Schlögl, R. The roles of subsurface carbon and hydrogen in palladium-catalyzed alkyne hydrogenation. *Science* **2008**, *320*, 86−89.
(19) Tew, M. W.; Nachtegaal, M.; Janousch, M.; Huthwelker, T.; van Bokhoven, J. A. The irreversible formation of palladium carbide during hydrogenation of 1-pentyne over silica-supported palladium nanoparticles: in situ Pd K and L_3 edge XAS. *Phys. Chem. Chem. Phys.* **2012**, *14*, 5761−5768.
(20) Teschner, D.; Borsodi, J.; Kis, Z.; Szentmiklósi, L.; Révay, Z.; Knop-Gericke, A.; Schlögl, R.; Torres, D.; Sautet, P. Role of hydrogen species in palladium-catalyzed alkyne hydrogenation. *J. Phys. Chem. C* **2010**, *114*, 2293−2299.
(21) (a) Flanagan, T. B.; Oates, W. A. The palladium-hydrogen system. *Annu. Rev. Mater. Sci.* **1991**, *21*, 269−304. (b) Flanagan, T. B.; Oates, W. A. The palladium-hydrogen system. *Annu. Rev. Mater. Sci.* **1991**, *21*, 269−304.
(22) Bugaev, A. L.; Guda, A. A.; Lomachenko, K. A.; Lazzarini, A.; Srabionyan, V. V.; Vitillo, J. G.; Piovano, A.; Groppo, E.; Bugaev, L. A.; Soldatov, A. V.; et al. Hydride phase formation in carbon supported palladium hydride nanoparticles by in situ EXAFS and XRD. *J. Phys.: Conf. Ser.* **2016**, *712*, 012032.
(23) Davis, R.; Landry, S.; Horsley, J.; Boudart, M. X-ray-absorption study of the interaction of hydrogen with clusters of supported palladium. *Phys. Rev. B: Condens. Matter Mater. Phys.* **1989**, *39*, 10580−10583.
(24) Tew, M. W.; Janousch, M.; Huthwelker, T.; van Bokhoven, J. A. The roles of carbide and hydride in oxide-supported palladium nanoparticles for alkyne hydrogenation. *J. Catal.* **2011**, *283*, 45−54.
(25) Vogel, W.; He, W.; Huang, Q.-H.; Zou, Z.; Zhang, X.-G.; Yang, H. Palladium nanoparticles "breathe" hydrogen; a surgical view with X-ray diffraction. *Int. J. Hydrogen Energy* **2010**, *35*, 8609−8620.
(26) (a) Bugaev, A. l.; Usoltsev, O. A.; Lazzarini, A.; Lomachenko, K. A.; Guda, A. A.; Pellegrini, R.; Carosso, M.; Vitillo, J.; Groppo, E.; van Bokhoven, J.; Soldatov, A. V.; Lamberti, C. Time-resolved operando studies of carbon supported Pd nanoparticles under hydrogenation reactions by X-ray diffraction and absorption. *Faraday Discus.* **2018**, Accepted Manuscript DOI: 10.1039/C7FD00211D. Chase, Z. A.; Fulton, J. L.; Camaioni, D. M.; Mei, D.; Balasubramanian, M.; Pham, V.-T.; Zhao, C.; Weber, R. S.; Wang, Y.; Lercher, J. A. State of supported Pd during catalysis in water. *J. Phys. Chem. C* **2013**, *117*, 17603−17612.
(27) Scarano, D.; Bordiga, S.; Lamberti, C.; Ricchiardi, G.; Bertarione, S.; Spoto, G. Hydrogen adsorption and spill-over effects on H-Y and Pd-containing Y zeolites: An experimental and theoretical investigation. *Appl. Catal., A* **2006**, *307*, 3−12.
(28) Srabionyan, V. V.; Bugaev, A. L.; Pryadchenko, V. V.; Avakyan, L. A.; van Bokhoven, J. A.; Bugaev, L. A. EXAFS study of size dependence of atomic structure in palladium nanoparticles. *J. Phys. Chem. Solids* **2014**, *75*, 470−476.
(29) Fajula, F. Methane and methanol synthesis over supported palladium catalysts. *J. Catal.* **1982**, *73*, 237−256.
(30) Nakamura, S. The mechanism of the palladium-catalyzed synthesis of vinyl acetate from ethylene in a heterogeneous gas reaction. *J. Catal.* **1970**, *17*, 366−374.
(31) Zaidi, S. Gas-phase acetoxylation of ethylene: Palladium-on-carbon catalyst stability. *J. Catal.* **1981**, *68*, 255−263.
(32) Armbrüster, M.; Behrens, M.; Cinquini, F.; Föttinger, K.; Grin, Y.; Haghofer, A.; Klötzer, B.; Knop-Gericke, A.; Lorenz, H.; Ota, A.; et al. How to control the selectivity of palladium-based catalysts in hydrogenation reactions: The role of subsurface chemistry. *ChemCatChem* **2012**, *4*, 1048−1063.
(33) Tew, M. W.; Miller, J. T.; van Bokhoven, J. A. Particle size effect of hydride formation and surface hydrogen adsorption of nanosized palladium catalysts: L_3 edge vs K edge X-ray absorption spectroscopy. *J. Phys. Chem. C* **2009**, *113*, 15140−15147.
(34) van Bokhoven, J. A.; Lamberti, C., Eds. *X-Ray Absorption and X-Ray Emission Spectroscopy: Theory and Applications*; John Wiley & Sons: Chichester (UK), 2016; Vol. *I, II*, pp 1−896.
(35) Bugaev, A. L.; Srabionyan, V. V.; Soldatov, A. V.; Bugaev, L. A.; van Bokhoven, J. A. The role of hydrogen in formation of Pd XANES in Pd-nanoparticles. *J. Phys.: Conf. Ser.* **2013**, *430*, 012028.
(36) Bordiga, S.; Groppo, E.; Agostini, G.; van Bokhoven, J. A.; Lamberti, C. Reactivity of surface species in heterogeneous catalysts probed by in situ X-ray absorption techniques. *Chem. Rev.* **2013**, *113*, 1736−850.
(37) Guda, A. A.; Guda, S. A.; Soldatov, M. A.; Lomachenko, K. A.; Bugaev, A. L.; Lamberti, C.; Gawelda, W.; Bressler, C.; Smolentsev, G.; Soldatov, A. V.; et al. Finite difference method accelerated with sparse solvers for structural analysis of the metal-organic complexes. *J. Phys.: Conf. Ser.* **2016**, *712*, 012004.
(38) Guda, S. A.; Guda, A. A.; Soldatov, M. A.; Lomachenko, K. A.; Bugaev, A. L.; Lamberti, C.; Gawelda, W.; Bressler, C.; Smolentsev, G.; Soldatov, A. V.; et al. Optimized finite difference method for the full-potential XANES simulations: Application to molecular adsorption geometries in MOFs and metal−ligand intersystem crossing transients. *J. Chem. Theory Comput.* **2015**, *11*, 4512−4521.
(39) Piovano, A.; Lazzarini, A.; Pellegrini, R.; Leofanti, G.; Agostini, G.; Rudić, S.; Bugaev, A. L.; Lamberti, C.; Groppo, E. Progress in the

DOI: 10.1021/acs.jpcc.7b11473
J. Phys. Chem. C 2018, 122, 12029−12037

characterization of the surface species in activated carbons by means of INS spectroscopy coupled with detailed DFT calculations. *Adv. Condens. Matter Phys.* **2015**, *2015*, 1−8.
(40) van Beek, W.; Safonova, O. V.; Wiker, G.; Emerich, H. SNBL, a dedicated beamline for combinedin situ X-ray diffraction, X-ray absorption and Raman scattering experiments. *Phase Transitions* **2011**, *84*, 726−732.
(41) Lamberti, C.; Bordiga, S.; Bonino, F.; Prestipino, C.; Berlier, G.; Capello, L.; D'Acapito, F.; Xamena, F. X. L. I.; Zecchina, A. Determination of the oxidation and coordination state of copper on different Cu-based catalysts by XANES spectroscopy in situ or in operando conditions. *Phys. Chem. Chem. Phys.* **2003**, *5*, 4502−4509.
(42) Ravel, B.; Newville, M. ATHENA, ARTEMIS, HEPHAESTUS: data analysis for X-ray absorption spectroscopy using IFEFFIT. *J. Synchrotron Radiat.* **2005**, *12*, 537−541.
(43) Zabinsky, S. I.; Rehr, J. J.; Ankudinov, A.; Albers, R. C.; Eller, M. J. Multiple-scattering calculations of X-ray-absorption spectra. *Phys. Rev. B: Condens. Matter Mater. Phys.* **1995**, *52*, 2995−3009.
(44) Kresse, G.; Furthmuller, J. Efficient iterative schemes for ab initio total-energy calculations using a plane-wave basis set. *Phys. Rev. B: Condens. Matter Mater. Phys.* **1996**, *54*, 11169−11186.
(45) Kresse, G.; Joubert, D. From ultrasoft pseudopotentials to the projector augmented-wave method. *Phys. Rev. B: Condens. Matter Mater. Phys.* **1999**, *59*, 1758−1775.
(46) Hafner, J. Ab-initio simulations of materials using VASP: Density-functional theory and beyond. *J. Comput. Chem.* **2008**, *29*, 2044−2078.
(47) Perdew, J. P.; Burke, K.; Ernzerhof, M. Generalized gradient approximation made simple. *Phys. Rev. Lett.* **1996**, *77*, 3865−3868.
(48) Methfessel, M.; Paxton, A. T. High-precision sampling for Brillouin-zone integration in metals. *Phys. Rev. B: Condens. Matter Mater. Phys.* **1989**, *40*, 3616−3621.
(49) Wyckoff, R. W. G.; Wyckoff, R. W., Eds. *Crystal structures*; Interscience: New York, 1960; Vol. *2*.
(50) Bunau, O.; Joly, Y. Self-consistent aspects of x-ray absorption calculations. *J. Phys.: Condens. Matter* **2009**, *21*, 345501.
(51) Smolentsev, G.; Soldatov, A. Quantitative local structure refinement from XANES: multi-dimensional interpolation approach. *J. Synchrotron Radiat.* **2006**, *13*, 19−29.
(52) Smolentsev, G.; Soldatov, A. V. FitIt: New software to extract structural information on the basis of XANES fitting. *Comput. Mater. Sci.* **2007**, *39*, 569−574.
(53) Langhammer, C.; Zhdanov, V. P.; Zorić, I.; Kasemo, B. Size-dependent kinetics of hydriding and dehydriding of Pd nanoparticles. *Phys. Rev. Lett.* **2010**, *104*, 135502.
(54) Martini, A.; Borfecchia, E.; Lomachenko, K. A.; Pankin, I. A.; Negri, C.; Berlier, G.; Beato, P.; Falsig, H.; Bordiga, S.; Lamberti, C. Composition-driven Cu-speciation and reducibility in Cu-CHA zeolite catalysts: a multivariate XAS/FTIR approach to complexity. *Chem. Sci.* **2017**, *8*, 6836−6851.
(55) Pappas, D. K.; Borfecchia, E.; Dyballa, M.; Pankin, I. A.; Lomachenko, K. A.; Martini, A.; Signorile, M.; Teketel, S.; Arstad, B.; Berlier, G.; et al. Methane to methanol: structure-activity relationships for Cu-CHA. *J. Am. Chem. Soc.* **2017**, *139*, 14961−14975.
(56) Stachurski, J.; Frackiewicz, A. A new phase in the Pd-C system formed during the catalytic hydrogenation of acetylene. *J. Less-Common Met.* **1985**, *108*, 249−256.
(57) Molnar, A.; Sarkany, A.; Varga, M. Hydrogenation of carbon-carbon multiple bonds: chemo-, regio- and stereo-selectivity. *J. Mol. Catal. A: Chem.* **2001**, *173*, 185−221.
(58) Gentle, T. M.; Muetterties, E. L. Acetylene, ethylene, and arene chemistry of palladium surfaces. *J. Phys. Chem.* **1983**, *87*, 2469−2472.
(59) Aleksandrov, H. A.; Moskaleva, L. V.; Zhao, Z.-J.; Basaran, D.; Chen, Z.-X.; Mei, D.; Rösch, N. Ethylene conversion to ethylidyne on Pd(111) and Pt(111): A first-principles-based kinetic Monte Carlo study. *J. Catal.* **2012**, *285*, 187−195.
(60) Bugaev, L. A.; Avakyan, L. A.; Srabionyan, V. V.; Bugaev, A. L. Resolution of interatomic distances in the study of local atomic structure distortions by energy-restricted x-ray absorption spectra. *Phys. Rev. B: Condens. Matter Mater. Phys.* **2010**, *82*, 064204.
(61) Bugaev, A. L.; Guda, A. A.; Lomachenko, K. A.; Kamyshova, E. G.; Soldatov, M. A.; Kaur, G.; Øien-Ødegaard, S.; Braglia, L.; Lazzarini, A.; Manzoli, M.; Bordiga, S.; Olsbye, U.; Lillerud, K. P.; Soldatov, A. V.; Lamberti, C. Operando study of palladium nanoparticles inside UiO-67 MOF for catalytic hydrogenation of hydrocarbons. *Faraday Discuss.* **2018**.
(62) (a) Chavan, S.; Vitillo, J. G.; Gianolio, G.; Zavorotynska, O.; Civalleri, B.; Jakobsen, S.; Nilsen, M. H.; Valenzano, L.; Lamberti, C.; Lillerud, K. L.; Bordiga, S. H2 storage in isostructural UiO-67 and UiO-66 MOFs. *Phys. Chem. Chem. Phys.* **2012**, *14*, 1614−1626. (b) Øien, S.; Agostini, G.; Svelle, S.; Borfecchia, E.; Lomachenko, K. A.; Mino, L.; Gallo, E.; Bordiga, S.; Olsbye, U.; Lillerud, K. P.; Lamberti, C. Probing Reactive Platinum Sites in UiO-67 Zirconium Metal-organic Frameworks. *Chem. Mater.* **2015**, *27*, 1042−1056.
(63) Safonova, O. V.; Tromp, M.; van Bokhoven, J. A.; de Groot, F. M.; Evans, J.; Glatzel, P. Identification of CO adsorption sites in supported Pt catalysts using high-energy-resolution fluorescence detection X-ray spectroscopy. *J. Phys. Chem. B* **2006**, *110*, 16162−16164.
(64) Singh, J.; Lamberti, C.; van Bokhoven, J. A. Advanced X-ray absorption and emission spectroscopy: in situ catalytic studies. *Chem. Soc. Rev.* **2010**, *39*, 4754−66.
(65) Timoshenko, J.; Lu, D.; Lin, Y.; Frenkel, A. I. Supervised machine-learning-based determination of three-dimensional structure of metallic nanoparticles. *J. Phys. Chem. Lett.* **2017**, *8*, 5091−5098.

DOI: 10.1021/acs.jpcc.7b11473
J. Phys. Chem. C 2018, 122, 12029−12037